Application of microscopic Förster resonance energy transfer to cytological diagnosis of the thyroid tumors

Shin-ichi Murata
University of Yamanashi
Interdisciplinary Graduate School of Medicine and Engineering
Department of Pathology
Yamanashi, Japan

Petr Herman
Charles University
Faculty of Mathematics and Physics
Prague, Czech Republic

Masanori Iwashina
Kunio Mochizuki
Tadao Nakazawa
Tetsuo Kondo
Nobuki Nakamura
University of Yamanashi
Interdisciplinary Graduate School of Medicine and Engineering
Department of Pathology
Yamanashi, Japan

Joseph R. Lakowicz
University of Maryland School of Medicine
Department of Biochemistry and Molecular Biology
Center for Fluorescence Spectroscopy
Baltimore, Maryland

Ryohei Katoh
University of Yamanashi
Interdisciplinary Graduate School of Medicine and Engineering
Department of Pathology
Yamanashi, Japan

Abstract. We propose a novel application of microscopic Förster resonance energy transfer (FRET) to clinical cytological diagnosis based on sensitive measurements of distance changes between fluorescently labeled deoxyribose nucleic acid (DNA) molecules. We have employed the microscopic FRET imaging for investigation of six papillary carcinomas and eight benign cases. In each case the FRET images of 20 cells stained by the AT-specific donor Hoechst 33258 and the GC-specific acceptor 7-aminoactinomycin D were acquired and analyzed by texture analysis. We have not found significant difference of the mean FRET efficiency between the benign and malignant groups. On the other hand, the texture analysis revealed a significant difference of the intranuclear spatial distribution of FRET efficiencies between the benign and malignant groups. The results indicate that despite the similar average distance between the AT- and the GC-rich DNA segments in the papillary carcinomas and the benign cases, the former has more heterogeneous distribution of the AT- and the GC-rich DNA segments in nuclei compared to the benign groups. We have demonstrated that the FRET imaging is a helpful tool for the medical cytological diagnosis of human tumors by giving information on the chromatin topology on the scale below the resolution of conventional optical microscopes. [DOI: 10.1117/1.1924667]

Keywords: thyroid; papillary carcinoma; FRET; cytology; morphometry; texture analysis.

Paper 04121 received Jul. 6, 2004; revised manuscript received Dec. 1, 2004; accepted for publication Dec. 2, 2004; published online May 24, 2005.

1. Introduction

Aspiration biopsy cytology of thyroid tumors is currently one of the most employed diagnostic methods for the differential diagnosis of malignant and benign lesions in the clinical medicine.[1,2] The cytological diagnosis of the thyroid lesions is based on the cellular atypia. These include the nuclear morphology such as the nuclear size, shape, and the chromatin pattern.[3–5] Since evaluation of the nuclear chromatin pattern is of a particular importance in the diagnosis of the thyroid papillary carcinoma (PC), significant work has been done to develop reliable method for differentiation between chromatin patterns of the PC and other thyroid lesions, including hyperplasia, adenoma and follicular carcinoma.[6–17] The majority of the studies have approached this issue by looking for changes of the local deoxyribose nucleic acid (DNA) concentration. However, characteristic chromatin patterns of the thyroid tumors are described not only by the local DNA concentration, but also by the DNA conformation and/or by the three-dimensional relationship between different chromosomes. This requires investigation of the structural and topological changes of the DNA on the angstrom scale. Förster resonance energy transfer (FRET) is a great tool for such distance measurements.[18]

We have reported on the cell cycle-related structural and topological changes in interphase nuclei of culture cells examined by the microscopic FRET method.[19,20] The FRET is a nonradiative process when the excited

Address all correspondence to Shin-ichi Murata, University of Yamanashi, Interdisciplinary Graduate School of Medicine and Engineering, Department of Pathology, 1110 Shimokato, Tamaho-cho, Nakakoma-gun, Yamanashi 409-3898 Japan. Tel: +81-55-273-9526; Fax: +81-55-273-9534; E-mail: smurata@yamanashi.ac.jp

1083-3668/2005/$22.00 © 2005 SPIE

fluorescent donor is transferred to the acceptor molecule.[18,21] Since the FRET efficiency depends on the inverse sixth power of the donor-acceptor distance, the FRET can be used as a highly sensitive ruler for measurements of intermolecular distances on the scale of 10–100 Å.[22–24] When used in microscopy, the microscopic FRET of samples specifically labeled by a proper donor-acceptor pair makes possible to extract information on distances below the diffraction limit, which are normally inaccessible by the optical microscopy. Therefore measurements of the distance change between segments of DNA molecules related to the structural and topological changes of the DNA are possible.[19,20,25,26]

In this paper, we present a novel medical application of our previous microscopic FRET work to the clinical cytological diagnosis of thyroid tumor cells.[19,20,24,26] We describe in more detail difference in the DNA organization between the papillary carcinoma and the follicular lesions of the thyroid by means of the microscopic FRET measurement between the AT-specific dye Hoechst 33258 (Ho) and the GC-specific dye 7-aminoactinomycin D (7-AAD). Results are interpreted in terms of the spatial proximity of the AT- and the GC-rich DNA regions. In order to quantitatively evaluate the FRET images, the two-dimensional maps of the corrected FRET signal were classified by the texture analysis.[27,28]

2. Materials and Methods

2.1 *Cytological Specimens and Fluorescence Staining*

Biological material was obtained from the files of the Kofu Municipal Hospital (Yamanashi, Japan). Touch smear cytology (TSC) specimens were prepared from the fresh sections taken from 14 patients with tumorous lesions by lobectomy or thyroidectomy. A group of the 14 Japanese patients included five male patients and nine female patients with mean age at diagnosis of 49.6 years. The histological diagnosis was done according to the WHO criteria. The 14 cases consisted of 6 papillary carcinomas (PCs), 6 adenomatous goiters (AGs), and 2 follicular adenomas (FAs). The TSC specimens were fixed in 90% ethanol (4 °C, at least 30 min). After a rinse, the cells were stained by 0.8 μM Ho and 1.6 μM 7-AAD, which were used as the donor and the acceptor, respectively. The donor-acceptor pair exhibited a good spectral match for the FRET experiments.[19,26] Ho and 7-AAD were obtained from the Molecular Probes (Eugene, OR). Other experimental details are described elsewhere.[19,20,26]

2.2 *Acquisition of FRET Images*

The steady state FRET microscopy with multiple acceptors can suffer from several sources of distortions including direct excitation of the acceptor at the donor excitation wavelengths and the dependence of FRET on the concentration of acceptor. Therefore we measured corrected FRET ($I_{c\mathrm{FRET}}$) signal using the Gordon's method [Eq. (1)]. The method is based on a usage of three fluorescence filter sets correcting data for cross talk, i.e., for detection of donor fluorescence with the acceptor emission filter and detection of acceptor fluorescence with the donor emission filter. The three filter sets were: (1) The donor filter set (*D*) consisting of the 360–370 nm excitation filter, the 400 nm dichroic mirror, and the 420–460 nm emission filter; (2) the acceptor filter set (*A*) consisting of the 530–550 nm excitation filter, the 590 nm dichroic mirror, and the 590 nm long-pass emission filter; (3) the FRET filter set (*F*) consisting of the 360–370 nm excitation filter, the 400 nm dichroic mirror, and the 590 nm long pass emission filter.[26,29] We acquired three fluorescence intensity images with the three filter sets in order to calculate the corrected energy transfer signal represented as the $-I_{c\mathrm{FRET}}$ image of each cell

$$I_{c\mathrm{FRET}}=\frac{F(da)-D(da)\dfrac{F(d)}{D(d)}-A(da)\dfrac{F(a)}{A(a)}}{G\cdot D(da)\cdot A(da)}. \qquad (1)$$

The term $F(da)$ is a fluorescence signal from cells double-stained with the donor and acceptor and collected with the filter set, *F*, $D(da)$ and $A(da)$ is a signal from the double-stained cells collected with the filter set *D* and *A*, respectively. Similarly, $F(d)$ and $D(d)$ is a signal from a donor-only stained cell using the filter set *F* and *D*, respectively. Finally, $F(a)$ and $A(a)$ is emission from the acceptor-only stained cell acquired with the filter set *F* and *A*, respectively. Ratios $F(d)/D(d)$ and $F(a)/A(a)$ are constant and depend on fluorophores and instrumentation only. We have used values $F(d)/D(d)=0.34$ and $F(a)/A(a)=0.03$. The ratios were measured with the donor-only and the acceptor-only stained cell, respectively. We have applied a constant scaling coefficient $G=10^{-6}$ to transform pixel values of the $I_{c\mathrm{FRET}}$ images to the 12 bit region.

The fluorescence intensity images were acquired on an epi-illuminant fluorescence microscope BX50 (Olympus, Tokyo, Japan) equipped with an UplanApo X40 oil immersion objective (numerical aperture=1.0) and a scientific-grade cooled charge coupled device (CCD) camera, Sensys (Photometrics, Tucson, AZ) connected to a personal computer. The images were pre-processed by the IPLab software (Scanalytics Inc., Fairfax, VA). The neutral-density filters were utilized to adjust an adequate illumination and minimize photobleaching.

At first, we have evaluated an amount of the nuclear DNA in the double-stained cells. The total acceptor fluorescence, proportional to the DNA content, has been used for selection of cells in the $G_{0/1}$ phases having the same amount of DNA as lymphocytic nuclei in the G_0 phase. The signal was collected with the filter set *A* in order to excite acceptor molecules only. Twenty cells of each tumor case have been selected. Then, three fluorescence intensity images of each cell, were measured using the *A*, *D*, and *F* filter sets and the $I_{c\mathrm{FRET}}$ images were constructed by pixel-by-pixel evaluation of the $I_{c\mathrm{FRET}}$ intensity from Eq. (1).

2.3 *Quantitative Analysis of the FRET Images*

To extract and compare characteristic features of cells from the papillary thyroid tumor and from the follicular lesions, the $I_{c\mathrm{FRET}}$ images were quantitatively analyzed by texture analysis. The total FRET signal was calculated in every nucleus as a sum of the pixel values. For the description of the image texture we have used the coefficient of variation (CV) and three parameters from the Haralick's method based on the co-occurrence matrix.[27,30] Specifically, we have chosen the angular second moment (ASM), which shows spatial homogeneity of the image, the sum variance (SVar), which reveals spatial heterogeneity, and the difference variance (DVar), which characterizes contrast of the $I_{c\mathrm{FRET}}$ image. These three

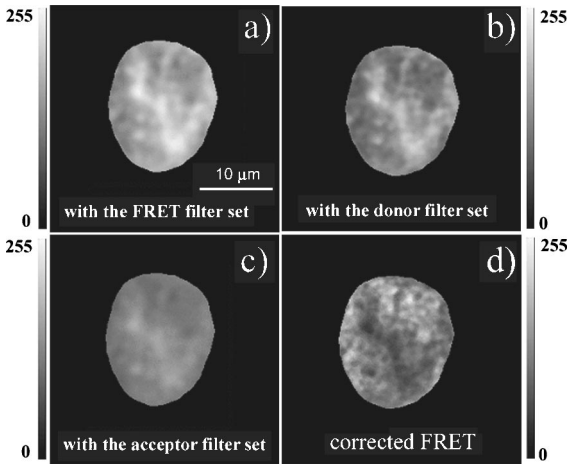

Fig. 1 Nuclear fluorescence intensity and I_{cFRET} images of a single cell double-stained by Ho and 7-AAD. (a) The fluorescence intensity image taken with the FRET filter set; (b) the fluorescence intensity image acquired with the donor filter set; (c) the fluorescence intensity image collected with the acceptor filter set; and (d) the I_{cFRET} image corrected by the Gordon's equation [Eq. (1)].

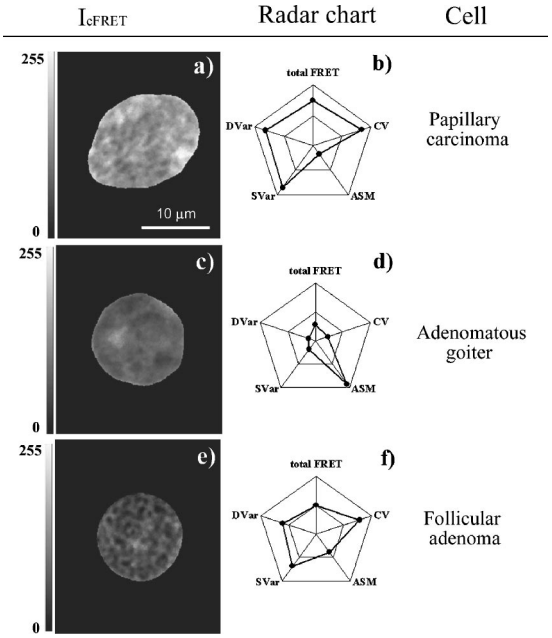

Fig. 2 Typical results obtained on a single cell of the papillary carcinoma [(a) and (b)], adenomatous goiter [(c) and (d)] and the follicular adenoma [(e) and (f)]. The I_{cFRET} images [(a),(c),(e)] were calculated from the Gordon's equation [Eq. (1)]. The radar charts show results of the quantitative texture analysis. The CV and the SVar are texture parameters characterizing the image heterogeneity, the ASM characterizes image homogeneity, and the DVar quantifies image contrast. The characteristic shape of the radar chart reflects spatial distribution of the FRET efficiency in the cell nucleus. All radar charts are presented in the same scale.

Haralick's parameters are independent from the size and shape of the cells, and describe pure texture features of the images.[16,17] The relevant co-occurrence matrix was constructed for every I_{cFRET} image after reduction of its bit depth from 12 to 8 bits. Equations used for calculation of the parameters have been described by Murata et al.[20] The four texture parameters served as mathematically independent descriptors of the I_{cFRET} images since they have been found to be sensitive enough to detect subtle changes of the DNA organization.[16,17,31]

In each case the case summary statistics was constructed from the mean value of the total FRET signal and from mean values of the texture parameters. The averaging was done over the 20 cells of the each case. The Mann-Whitney U test was applied to compare benign and malignant cancer groups and distinguish between them.

3. Results

Representative fluorescence intensity images of a nucleus from a single papillary carcinoma cell double-stained by Ho and 7-AAD taken with the *F*, *D*, and *A* filter sets are shown in Figs. 1(a), 1(b), and 1(c), respectively. The I_{cFRET} image calculated from the intensity images (a)–(c), and representing the corrected FRET signal is shown in Fig. 1(d). The I_{cFRET} image exhibits considerable spatial heterogeneity of the fluorescence energy transfer that indicates uneven spatial distribution of the donor-acceptor distances. Consequently, the image reports on an uneven separation of the AT- and GC-rich DNA segments in these locations. The bright and dark regions in the I_{cFRET} images correspond to high and low efficiency of the energy transfer, respectively.

Typical I_{cFRET} images of nuclei from single cells extracted from the papillary carcinoma, adenomatous goiter, and the follicular adenoma are presented in Figs. 2(a), 2(c), and 2(e), respectively. Visually inspected, the images reveal different distribution of the FRET efficiency in the nuclei. The I_{cFRET} image of the papillary cell exhibits highly heterogeneous FRET pattern whereas, the image of the adenomatous goiter cell is homogeneous. The I_{cFRET} image of the follicular adenoma cell shows granular spatial distribution of the FRET signal. This heterogeneity, however, seems to be lower than that of the PC cell, Fig. 2(a). Moreover, the cell nuclei seem to display a different total FRET signal, as judged by the overall brightness of the I_{cFRET} images.

To quantitatively support conclusions of the visual examination, we have performed the texture analysis of the I_{cFRET} images and quantification of the total FRET signal. Results of the texture analysis and values of the total FRET signal are shown in radar charts in Figs. 2(b), 2(d), and 2(f). The total FRET reports on the extent of the three-dimensional condensation of the AT- and the GC-rich DNA segments in the nuclei. The calculated texture coefficients provide a quantitative evaluation of the spatial heterogeneity, homogeneity, and contrast of the I_{cFRET} images. In particular, the CV and the SVar are texture parameters characterizing the image heterogeneity, the ASM characterizes image homogeneity, and the DVar quantifies image contrast. Mean values of the texture parameters averaged over 20 cells in each case were used for the case summary statistics, where we have compared characteristics of the PC, AG, and FA. Figure 3 shows distribution of the average total FRET signal for the individual cases. In parenthesis are given characteristic values calculated by averaging the plotted values over the cases in each group. Although the PC cases exhibit somehow higher values of the total FRET, there was not found significant difference of total

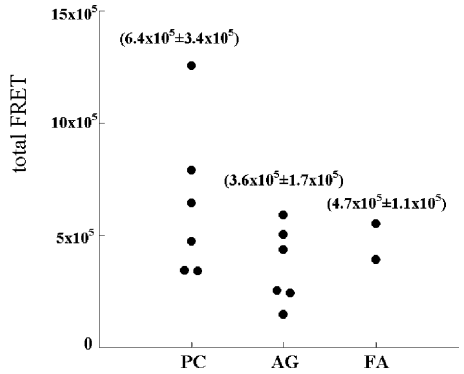

Fig. 3 Scatter graph of the total FRET signal in the PC, the AD, and the FC cells. Each data point represents a mean value calculated from 20 nuclei of one case. Means calculated over all cases in each group are given in parenthesis.

FRET signal between benign and malignant tumor groups after averaging these values over the whole group. Neither the ASM, describing image homogeneity, nor the DVar, describing the image contrast, revealed significant difference between the tumor groups, Figs. 4(b) and 4(d). Fortunately, values of the CV and SVar, which describe image heterogeneity, exhibited significant difference (CV, $p<0.02$; SVar, $p<0.04$) between the groups, suggesting possibility to distinguish the malignant papillary carcinoma from the adenomatous goiters and follicular adenomas, Figs. 4(a) and 4(c).

The results of the quantitative analysis suggest that the papillary carcinomas and follicular tumors have on average similar distance between the AT- and the GC-rich DNA segments. The papillary carcinomas, however, exhibit more heterogeneous distribution of the FRET efficiency in the nucleus than the adenomatous goiters and the follicular adenomas.

4. Discussion

The characteristic nuclear chromatin pattern of the papillary thyroid carcinomas is regarded as a criterion for the cytological diagnosis.[4,32,33] Previously, we have quantitatively investigated the chromatin pattern of thyroid tumor cells by the texture analysis. Difference in the spatial distribution of the nuclear DNA between the thyroid carcinoma and benign tumor cells have been reported.[11,16,17] The chromatin pattern of tumor cells originates from the DNA conformation, which depends on chromosome territories, the DNA concentration and condensation, the transcription activity, and the spatial correlation between the heterochromatin and the euchromatin. Specifically, the spatial correlation between the heterochromatin and the euchromatin in the nuclei is an important diagnostic marker in the cytological specimens.[4] The transcriptionally inactive heterochromatin contains the AT-rich DNA, whereas the transcriptionally active euchromatin consists mainly of the GC-rich DNA.[34] To extend our previous studies, we have used FRET technique to analyze the DNA organization on its molecular level, i.e., on the scale below the diffraction limit of the conventional optical microscopes.[19,20,26]

The unique property of FRET is its ability to measure molecular distances on the scale of tens of angstroms. An improved sensitivity of CCD cameras makes measurements of FRET under microscopes possible.[21,24,35] At present, the microscopic FRET is widely utilized for number of applications in biology and medicine.[21,23,36] Nevertheless, only a few FRET studies of the DNA organization in the interphase nuclei were reported.[25,37] Recently we have studied the cell-

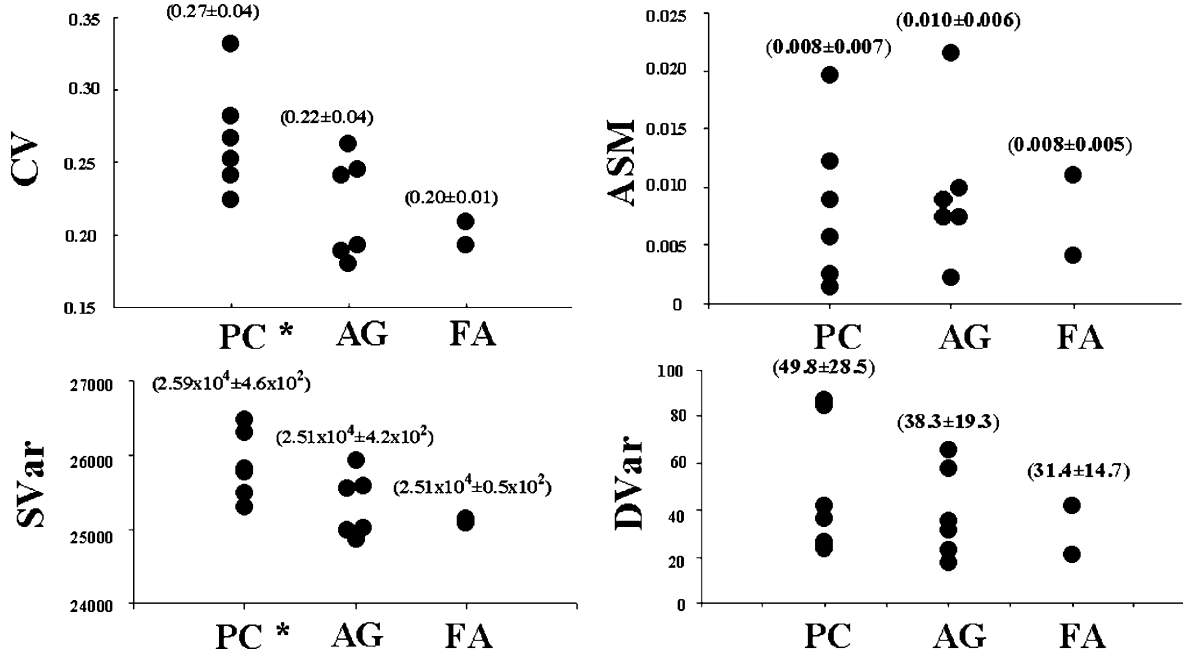

Fig. 4 Scatter graphs of the texture parameters calculated from the I_{cFRET} images of cells from the PC, AG, and FA. Each circle represents mean value of the CV, ASM, SVar, and DVar in one case. Mean calculated over all cases in each group are given in parenthesis. (*: PC versus AG and FA: CV, $p<0.02$; SVar, $p<0.04$.)

cycle dependent changes of the spatial distribution and the organization of the AT- and the GC-rich nuclear DNA regions in culture cells. Experiments were based on the microscopic FRET measurements using both the fluorescence intensity and the fluorescence lifetime imaging.[20,26,31] We have shown a difference between the microscopic FRET measurements with and without the Gordon's correction.[26] It was shown that the uncorrected FRET images were influenced not only by the donor-acceptor distance, but by the concentration of the donor as well. The corrected FRET efficiency was affected only by a variation of the distance between the AT- and the GC-rich DNA.

In this study, we have employed the corrected FRET measurement for estimation of the DNA topology unaffected by the local difference in the DNA condensation. Because all tumor cells were measured in the $G_{0/1}$ phases, we can eliminate an influence of the cell-cycle related change of the DNA organization. We have not found significant difference of the overall FRET efficiency between the benign and the malignant tumor groups. This suggests that the papillary carcinomas and the follicular tumors have on average similar distance between the AT- and the GC-rich DNA segments. Since the FRET signal calculated by the Gordon's equation is not rigorously equal to the real FRET efficiency, we have to note that the high average $I_{c\mathrm{FRET}}$ values found in the few PC cases might not be related to an extremely large change of the DNA topology. On the other hand, the quantitative analysis of as few as 20 cells of the each case reveals that the papillary carcinomas exhibit more heterogeneous distribution of the total FRET signal in the nucleus than the adenomatous goiters and the follicular adenomas. As shown in Fig. 4, some papillary carcinoma cases exhibit overlapped parameters with adenomatous goiters, which can be troubling in the clinical application. In this study, however, we have demonstrated that the corrected FRET measurement of as few as 20 cells can give valuable information for detection of the tumorous changes in the DNA topology, that has been so far inaccessible by the conventional steady-state fluorescence microscopy. Due to a limed number of cases available for this study we do not propose to use the corrected FRET method as an exclusive tool for detection of the tumorous changes in the DNA topology. This would certainly require careful examination of much larger ensemble of cases. However, characteristic chromatin feature of the papillary carcinoma cells revealed by the corrected FRET method can add significant information to the ordinary cytological findings such as nuclear size, shape, and conventional chromatin patterns.

In conclusion, we have demonstrated that the corrected FRET imaging is a helpful tool for the clinical cytological diagnosis of human tumors by giving additional information on the characteristic chromatin patterns.

References

1. K. C. Suen, ''Fine-needle aspiration biopsy of the thyroid,'' *CMAJ* **167**, 491–495 (2002).
2. I. A. El Hag, S. M. Kollur, and L. C. Chiedozi, ''The role of FNA in the initial management of thyroid lesions: 7-year experience in a district general hospital,'' *Cytopathology* **14**, 126–130 (2003).
3. W. Frable and M. Frable, ''Fine-needle biopsy of the thyroid: histolopathologic and clinical correlations,'' in *In Progress in Surgical Pathology*, M. W. Cm Fenoglio, Eds., pp. 105–118, Masson, New York (1980).
4. G. L. Koss and J. Zajicek, ''The thyroid,'' in *Diagnostic Cytology and Its Histopathologic Bases*, G. L. Koss, Ed., pp. 1268–1279, Lippincott Williams & Wilkins, Philadelphia (1992).
5. K. T. Mai, H. M. Yazdi, A. S. Commons, D. G. Perkins, and L. Macdonald, ''Neoplastic non-papillary thyroid carcinoma lesions with a fine chromatin pattern,'' *Pathol. Int.* **49**, 601–607 (1999).
6. M. E. Boon, T. Lowhagen, P. L. Cardozo, D. I. Blonk, P. J. Kurver, and J. P. Baak, ''Computation of preoperative diagnosis probability for follicular adenoma and carcinoma of the thyroid on aspiration smears,'' *Anal Quant Cytol.* **4**, 1–5 (1982).
7. A. Kriete, R. Schaffer, H. Harms, and H. M. Aus, ''Computer-based cytophotometric classification of thyroid tumors in imprints,'' *J. Cancer Res. Clin. Oncol.* **109**, 252–256 (1985).
8. M. Bibbo, P. H. Bartels, H. Galera-Davidson, H. E. Dytch, and G. L. Wied, ''Markers for malignancy in the nuclear texture of histologically normal tissue from patients with thyroid tumors,'' *Anal Quant Cytol. Histol.* **8**, 168–176 (1986).
9. S. Murata, Y. Urata, M. Kamachi, N. Morotomi, Y. Tsuchihasi, F. Matsuzuka, K. Kuma, and T. Ashihara, ''Cytofluorometric analysis of cell kinetics and nuclear ploidy patterns of thyroid tumor,'' *Pathology and Clinical Medicine* **7**, 1009–1016 (1989).
10. O. Ferrer-Roca, E. Ballester-Guardia, and J. Martin, ''Nuclear chromatin texture to differentiate follicular and papillary carcinoma of the thyroid,'' *Pathol. Res. Pract.* **185**, 561–566 (1989).
11. S. Murata, ''Correlated analysis of nuclear DNA content and nuclear morphological features in the thyroid hyperplasias and tumors using image cytometry,'' *J. Kyoto Pref. Univ. Med.* **100**, 311–331 (1991).
12. I. Salmon, R. Kiss, B. Franc, P. Gasperin, R. Heimann, J. L. Pasteels, and A. Verhest, ''Comparison of morphonuclear features in normal, benign and neoplastic thyroid tissue by digital cell image analysis,'' *Anal Quant Cytol. Histol.* **14**, 47–54 (1992).
13. O. Ferrer-Roca, J. A. Perez Gomez, and M. Estevez, ''Chromatin texture from hematoxylin stained thyroid lesions,'' *Anal Cell Pathol.* **17**, 209–217 (1998).
14. V. A. Kirillov, Y. P. Yuschenko, A. A. Paplevka, and E. P. Demidchik, ''Thyroid carcinoma diagnosis based on a set of karyometric parameters of follicular cells,'' *Cancer* **92**, 1818–1827 (2001).
15. H. Harms, M. Hofmann, and I. Ruschenburg, ''Fine needle aspiration of the thyroid: can an image processing system improve differentiation?,'' *Anal Quant Cytol. Histol.* **24**, 147–153 (2002).
16. S. Murata, K. Mochizuki, T. Nakazawa, T. Kondo, N. Nakamura, H. Yamashita, Y. Urata, T. Ashihara, and R. Katoh, ''Detection of underlying characteristics of nuclear chromatin patterns of thyroid tumor cells using texture and factor analyses,'' *Cytometry* **49**, 91–95 (2002).
17. S. Murata, K. Mochizuki, T. Nakazawa, T. Kondo, N. Nakamura, H. Yamashita, Y. Urata, T. Ashihara, and R. Katoh, ''Morphological abstraction of thyroid tumor cell nuclei using morphometry with factor analysis,'' *Microsc. Res. Tech.* **61**, 457–462 (2003).
18. T. Forster, ''Intermolecular energy migration and fluorescence (Translated by R. S. Knox, Department of Physics and Astronomy, University of Rochester, Rochester, NY 14627),'' *Ann. Phys.* **2**, 55–75 (1948).
19. S. Murata, P. Herman, H.-J. Lin, and J. Lakowicz, ''Fluorescence lifetime imaging of nuclear DNA; effect of fluorescence resonance energy transfer,'' *Cytometry* **41**, 178–185 (2000).
20. S. Murata, P. Herman, and J. Lakowicz, ''Texture analysis of fluorescence lifetime images of nuclear DNA with effect of fluorescence resonance energy transfer,'' *Cytometry* **43**, 94–100 (2001).
21. J. Lakowicz, *Principles of Fluorescence Spectroscopy*, Kluwer Academic/Plenum, New York (1999).
22. L. Stryer, ''Fluorescence energy transfer as a spectroscopic ruler,'' *Annu. Rev. Biochem.* **47**, 819–846 (1978).
23. T. Jovin and D. Arndt-Jovin, ''FRET microscopy: digital imaging of fluorescence resonance energy transfer. Application in cell biology.9,'' in *Cell Structure and Function by Microspectrofluorometry*, E. Kohen, J. S. Ploem, and J. G. Hirschberg, Eds., pp. 99–117, Academic, Orlando (1989).
24. S. Murata, J. Kusba, G. Piszczek, I. Gryczynski, and J. Lakowicz, ''donor fluorescence decay analysis for energy transfer in double-helical DNA with various acceptor concentration,'' *Biopolymers* **57**, 306–315 (2000).
25. G. Bottiroli, A. C. Croce, G. Gerzeli, and S. Barni, ''DNA double staining for a fluorescence energy transfer study of chromatin in liver cells,'' *Cell Biophys.* **15**, 249–263 (1989).
26. S. Murata, P. Herman, K. Mochizuki, T. Nakazawa, T. Kondo, N. Nakamura, J. Lakowicz, and R. Katoh, ''Spatial distribution analysis

of AT- and GC-rich regions in nuclei using corrected fluorescence resonance energy transfer,'' *J. Histochem. Cytochem.* **51**, 951–958 (2003).
27. R. M. Haralick, K. Shanmugam, and I. Dinstein, ''Texture features for image classification,'' *IEEE Trans. Syst. Man Cybern.* **SMC3**, 610–621 (1973).
28. Y. Tzay and F. U. King-Sun, ''Texture analysis,'' in *Handbook of Pattern Recognition and Image Processing*, pp. 259–261, Academic, New York (1986).
29. G. W. Gordon, G. Berry, X. H. Liang, B. Levine, and B. Herman, ''Quantitative fluorescence resonance energy transfer measurements using fluorescence microscopy,'' *Biophys. J.* **74**, 2702–2713 (1998).
30. R. M. Haralick, ''Texture,'' in *Computer and Robot vision*, R. M. Haralick and L. Shapiro, Eds., pp. 453–507, Addison Wesley, New York (1992).
31. S. Murata, P. Herman, and J. Lakowicz, ''Texture analysis of fluorescence lifetime images of AT- and GC-rich regions in nuclei,'' *J. Histochem. Cytochem.* **49**, 1443–1452 (2001).
32. S. Kini, J. Miller, and J. Hamburgger, ''The cytopathology of papillary carcinoma of the thyroid by fine needle aspiration,'' *Acta Cytol.* **24**, 511–521 (1980).
33. T. Lowhagen and E. Sprenger, ''Cytologic presentation of thyroid tumours in aspiration biopsy smear. A review of 60 cases,'' *Acta Cytol.* **18**, 192–197 (1974).
34. B. Alberts, D. Bray, J. Lewis, M. Raff, K. Roberts, and J. D. Watson, *Molecular Biology of the Cell*, Garland, New York (1994).
35. J. R. Lakowicz, H. Szmacinski, K. Nowaczyk, K. W. Berndt, and M. Johnson, ''Fluorescence lifetime imaging,'' *Anal. Biochem.* **202**, 316–330 (1992).
36. J. Szollosi, P. Nagy, Z. Sebestyen, S. Damjanovicha, J. Park, and L. Matyus, ''Applications of fluorescence resonance energy transfer for mapping biological membranes,'' *J. Biotechnol.* **82**, 251–266 (2002).
37. E. Prosperi, M. C. Giangare, and G. Bottiroli, ''DNA stainability with base-specific fluorochromes: dependence on the DNA topology *in situ*,'' *Histochemistry* **102**, 123–128 (1994).